applied sciences

MDPI

Article

Heat Transfer of Nanomaterial over an Infinite Disk with Marangoni Convection: A Modified Fourier's Heat Flux Model for Solar Thermal System Applications

Mahanthesh Basavarajappa [1], Giulio Lorenzini [2,*], Srikantha Narasimhamurthy [3], Ashwag Albakri [4] and Taseer Muhammad [5]

1 Center for Mathematical Needs, Department of Mathematics, CHRIST (Deemed to be University), Bengaluru 560029, India; mahanthesh.b@christuniversity.in
2 Department of Engineering and Architecture, University of Parma, Parco Area Delle Scienze 181/A, 43124 Parma, Italy
3 Department of Mathematics, MS Ramaiah Institute of Technology, Bengaluru 560054, India; srikanthan@msrit.edu
4 Department of Computer Science, College of Computer Science & Information Technology, Jazan University, Jazan 45142, Saudi Arabia; aoalbakri@jazanu.edu.sa
5 Department of Mathematics, College of Sciences, King Khalid University, Abha 61413, Saudi Arabia; tasgher@kku.edu.sa
* Correspondence: giulio.lorenzini@unipr.it

Citation: Basavarajappa, M.; Lorenzini, G.; Narasimhamurthy, S.; Albakri, A.; Muhammad, T. Heat Transfer of Nanomaterial over an Infinite Disk with Marangoni Convection: A Modified Fourier's Heat Flux Model for Solar Thermal System Applications. *Appl. Sci.* **2021**, *11*, 11609. https://doi.org/10.3390/app112411609

Academic Editor: Alireza Dehghanisanij

Received: 30 September 2021
Accepted: 30 November 2021
Published: 7 December 2021

Abstract: The demand for energy due to the population boom, together with the harmful consequences of fossil fuels, makes it essential to explore renewable thermal energy. Solar Thermal Systems (STS's) are important alternatives to conventional fossil fuels, owing to their ability to convert solar thermal energy into heat and electricity. However, improving the efficiency of solar thermal systems is the biggest challenge for researchers. Nanomaterial is an effective technique for improving the efficiency of STS's by using nanomaterials as working fluids. Therefore, the present theoretical study aims to explore the thermal energy characteristics of the flow of nanomaterials generated by the surface gradient (Marangoni convection) on a disk surface subjected to two different thermal energy modulations. Instead of the conventional Fourier heat flux law to examine heat transfer characteristics, the Cattaneo–Christov heat flux (Fourier's heat flux model) law is accounted for. The inhomogeneous nanomaterial model is used in mathematical modeling. The exponential form of thermal energy modulations is incorporated. The finite-difference technique along with Richardson extrapolation is used to treat the governing problem. The effects of the key parameters on flow distributions were analyzed in detail. Numerical calculations were performed to obtain correlations giving the reduced Nusselt number and the reduced Sherwood number in terms of relevant key parameters. The heat transfer rate of solar collectors increases due to the Marangoni convection. The thermophoresis phenomenon and chaotic movement of nanoparticles in a working fluid of solar collectors enhance the temperature distribution of the system. Furthermore, the thermal field is enhanced due to the thermal energy modulations. The results find applications in solar thermal exchanger manufacturing processes.

Keywords: solar thermal exchangers; modified Fourier heat flux law; nanofluid; Marangoni convection; disk; thermal energy modulations

1. Introduction

Solar thermal energy plays a significant role in meeting the growing energy demand and in overcoming the consequences caused by the use of fossil fuels. Therefore, improving the thermal energy (performance) of solar heat exchangers is one of the key challenges in energy saving, energy use, and design. Researchers have established a new technique (using nanomaterials as functional fluids) to improve the efficiency of solar thermal systems.

Working fluids carrying nanoparticles composed of metal, metal oxides, and carbons result in a suspension called a nanofluid. The factors influencing the thermal energy characteristics of nanomaterials are their thermophysical characteristics, such as thermal conductivity, electrical conductivity, viscosity, heat capacity, and density. Choi [1] conducted a comprehensive study on nanomaterials and concluded that nanomaterials possess superior thermal characteristics. Khanafer et al. [2] proposed a homogeneous single-phase model to explore the phenomenon of heat transport by convection. Subsequently, Buongiorno [3] presented a heterogeneous model highlighting the importance of thermophoresis and the mechanisms of Brownian motion. Nield and Kuznetsov [4] studied the flow of nanomaterials on a plate using the Buongiorno model. Recently, the thermodynamic characteristics of nanomaterials on the surfaces of rotating discs have acquired great attention due to their extensive use in heat exchangers and solar thermal systems. Further work on nanomaterials can be seen in [5–10].

The study of non-Newtonian materials has been of extreme importance amongst industries and researchers owing to their applications in engineering areas such as fiber optic manufacturing, chemical manufacturing, petroleum industries, and industrial polymer industries. Non-Newtonian material flows are generally non-linear and do not conform to Navier–Stokes relations. In the early twentieth century, many researchers, Skelland [11], Denn [12], Rajagopal et al. [13], and Eldabe et al. [14], began theoretical research on non-Newtonian materials, now receiving special attention from areas such as radial diffuser design and thermal oil recovery, drag reduction, and others. The Casson fluid model fits most rheological data for many materials. The flow of the time-dependent surface layer dynamics of a Casson material on a movable plate was investigated by Mustafa et al. [15]. Nadem et al. [16] studied the consequence of the Lorentz force on the heat and flow of a Casson material using the Adomian decomposition (ADM) method. Eldabe [17] simulated the flow of non-Newtonian Casson material amongst two rotating cylinders with a radially imposed magnetic field. Gireesha et al. [18] performed numerical computations of heat transfer in the Casson material subjected to the Lorentz force. Mahanthesh et al. [19] explored the consequence of exponential heat source and cross-diffusion in the Casson material dynamics generated by the surface tension. Sohail et al. [20] discussed the momentum, concentration, and thermal diffusion in the surface layer magneto-flow of the Casson material in an elongated plate. Other studies related to the Casson material can be found in ([21–23]).

In the mid-1860s, Marangoni discovered the phenomenon that in natural convection, the gravity of the liquid predominated and gradually disappeared in conditions of microgravity. At the liquid interface, surface tension plays a significant role in the surface tension gradient. The growth of molten crystals, the growth of vapor bubbles during nucleation, semiconductor processing, and thin-film diffusion are some of the applications of Marangoni convection. It is also shown experimentally and numerically that there is a significant influence on heat transfer under microgravity conditions and it can also be on Earth's gravity [24]. Pearson [25] gave rise to the modeling of the Marangoni effect. Lin et al. [26] examined heat transport in a non-Newtonian material with a Marangoni convection-induced flow and an imposed thermal energy gradient. Ibrahim [27] deliberates on the convective dynamics of Marangoni with thermal radiation and mass injection. Mahanthesh et al. [28] analyzed the SWCNT and MWCNT nanoliquid flow caused by a disc with an irregular heat source and Lorentz force. Mahanta et al. [29] discussed the Marangoni convection in the Casson material flow created by an elongated plate. Shafiq et al. [30] conducted the study on the chemical reaction in the Marangoni convective flow over the Riga plate. Kármán [31] pioneered the work with rotating discs by adopting new variables and obtaining theoretical results for both laminar and turbulent flows. The Kármán [31] problem has been protracted by Turkyilmazoglu [32,33] to the case where the dynamics are considered in a rotating disk that stretches and contracts radially under magnetism. Makinde et al. [34] deliberated the stimulation of the exponential form of the heat source (ESHS) in the dynamics of the magneto-nanofluids generated by the elongation of the rotating disk surface. Numerical computations of Maxwell material driven by a spinning disc subjected to the thermophoresis and Cattaneo–Christov theory was carried out by Shehzad et al. [35]. Many authors, such as Rasool et al. [36] and Rashid et al. [37], contributed to the study of Marangoni's convective flow. However, the Marangoni convection in Casson material flow generated by disk surface is limited.

Although Fourier's law of conduction has various practical applications, the main limiting case of this model is that it provides an energy equation of parabolic nature, in which the system will be instantaneously affected by the initial disturbance. Cattaneo [38] overcomes this paradox. Cattaneo, in his model, modified the Fourier model considering the relaxation time for the heat flux. Later, Christov [39] introduced an invariant material form of the Cattaneo model, then Straughan [40] used the Cattaneo–Christov model (CCM) in his work to study thermal convection in laminar flow. Khan et al. [41] considered the heat transport in upper convected Maxwell fluid flow above the exponential form of an elongated surface by accounting for the CCM. Khan and Alzahrani [42] used the CCM in the magnetodynamics of non-Newtonian fluids and studied the characteristics of heat transport. Gireesha et al. [43] examined the magnetodynamics of Casson particulate fluid on the surface of a stretched plate taking into account the CCM for thermal energy analysis. Kareem et al. [44] explored the axisymmetric dynamics of third-degree fluids through porous media by implementing the CCM. However, the problems concerning the significance of CCM on the Marangoni convection driven by disk surface are very limited.

Given the literature survey, the main purpose is to investigate the thermal energy features of the flow of nanomaterials with Marangoni convection around an infinite disk with the exponential form of the thermal energy modulations. The disk surface temperature is assumed to be a quadratic function of the radial coordinate and heat sources are also taken into account. The CCM is used to govern the energy equation of the flow problem. The main novelty of the study is the application of the modified Fourier heat flow model in the Marangoni convection of nanomaterials. Numerical solutions are discussed graphically using 2D curves, surface graphs, and columns. Different types of mathematical models are proposed for the local heat and mass transfer rates. The statistical components of the fictitious model are discussed.

2. Mathematical Formulation

2.1. Conceptual Model

It is considered a flow of magneto-Casson-nanoliquid over an infinite disk with surface tension. The physical model comprising of a cylindrical coordinate system (r, φ, z) is shown in Figure 1. The flow is symmetric to the $z = 0$ plane and axisymmetric about the z-axis with $\partial/\partial\varphi = 0$ for all variables which is motivated by a surface tension due to the surface temperature/nanoparticle volume fraction gradient, which is known as the Marangoni layer. The flow is assumed to be steady, laminar, and irrotational, while the fluid is incompressible, and electrically conducting. The magnetic field is applied along z-direction. The disk surface is maintained with variable surface temperature T_w and variable surface nanoparticles volume fraction C_w, while both nanoparticle volume fraction and temperature are constant at the free surface. The physical properties of the fluid are assumed to be constant. The Prandtl's boundary layer and Boussinesq approximations are accounted. The two-phase Buongiorno model comprising of haphazard movement and thermophoresis mechanism of nanoparticles is implemented. The CCM is accounted to describe heat and mass transfer. Two different modulations of thermal energy are deliberated, such as the exponential special heat source (ESHS) and the thermal heat source (THS).

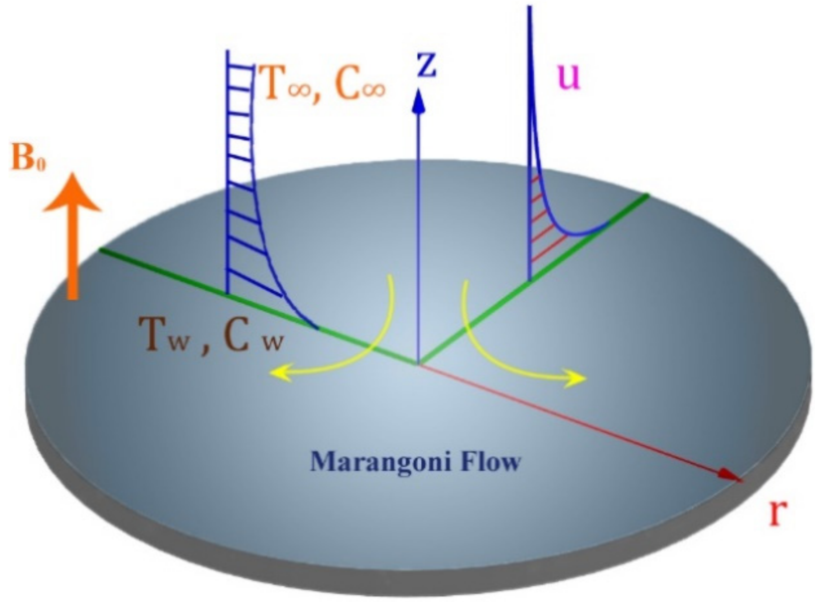

Figure 1. Physical model.

2.2. Governing Equations

The governing surface layer equations are (see [8–10]):

Conservation of mass

$$\frac{\partial u}{\partial r}+\frac{u}{r}+\frac{\partial w}{\partial z}=0, \tag{1}$$

Conservation of momentum

$$u\frac{\partial u}{\partial r}+w\frac{\partial u}{\partial z}=\frac{\mu}{\rho}\left(1+\frac{1}{\beta_c}\right)\frac{\partial^2 u}{\partial z^2}-\frac{\delta B_0^2}{\rho}u, \tag{2}$$

Conservation of thermal energy

$$\begin{aligned}&u\tfrac{\partial T}{\partial r}+w\tfrac{\partial T}{\partial z}+\lambda_T\left[u^2\tfrac{\partial^2 T}{\partial r^2}+w^2\tfrac{\partial^2 T}{\partial z^2}+2uw\tfrac{\partial^2 T}{\partial r\partial z}+\tfrac{\partial T}{\partial r}\left(u\tfrac{\partial u}{\partial r}+w\tfrac{\partial u}{\partial z}\right)+\tfrac{\partial T}{\partial z}\left(u\tfrac{\partial w}{\partial r}+w\tfrac{\partial w}{\partial z}\right)\right]\\&=\tfrac{k}{\rho c_p}\tfrac{\partial^2 T}{\partial z^2}+\tau\left\{D_B\tfrac{\partial T}{\partial z}\tfrac{\partial C}{\partial z}+\tfrac{D_T}{T_\infty}\left(\tfrac{\partial T}{\partial z}\right)^2\right\}+\tfrac{Q_e(T_w-T_\infty)}{\rho c_p}\exp\left\{-n\sqrt{\Omega/\nu}\,z\right\}+\tfrac{Q_t}{\rho c_p}(T-T_\infty),\end{aligned} \tag{3}$$

Conservation of nanoparticles volume fraction

$$\begin{aligned}&u\tfrac{\partial C}{\partial r}+w\tfrac{\partial C}{\partial z}=D_B\tfrac{\partial^2 C}{\partial z^2}+\tfrac{D_T}{T_\infty}\tfrac{\partial^2 T}{\partial z^2}\\&-\lambda_c\left[u^2\tfrac{\partial^2 C}{\partial r^2}+w^2\tfrac{\partial^2 C}{\partial z^2}+2uw\tfrac{\partial^2 C}{\partial r\partial z}+\tfrac{\partial C}{\partial r}\left(u\tfrac{\partial u}{\partial r}+w\tfrac{\partial u}{\partial z}\right)+\tfrac{\partial C}{\partial z}\left(u\tfrac{\partial w}{\partial r}+w\tfrac{\partial w}{\partial z}\right)\right],\end{aligned} \tag{4}$$

Boundary conditions

$$\begin{aligned}&\mu\left(1+\tfrac{1}{\beta_c}\right)\tfrac{\partial u}{\partial z}=\tfrac{\partial \sigma}{\partial r}=\tfrac{\partial \sigma}{\partial T}\tfrac{\partial T}{\partial r}+\tfrac{\partial \sigma}{\partial C}\tfrac{\partial C}{\partial r},\quad w=0,\\&T=T_w=T_\infty+A\left(\tfrac{r}{\Re}\right)^2\text{ and }C=C_w=C_\infty+B\left(\tfrac{r}{\Re}\right)^2\text{ at }z=0\\&u\to 0,\ T\to T_\infty,\ C\to C_\infty\text{ at }z\to\infty\end{aligned} \tag{5}$$

The second term on the right side of Equation (2) represents the transverse magnetic field, and the second and third terms on the right-hand side of Equation (3) represent the Brownian motion and Thermophoresis phenomenon. The thermophoresis parameter is quantified by nanoparticles particle's thermos-diffusion coefficient D_T and it signifies the capability of nanoparticles to move as a result of the temperature gradient. $D_T > 0$ signifies the movement of nanoparticles toward cooler regions while $D_T < 0$ designates the movement of nanoparticles toward warmer regions. The last two terms of Equation (3) represent the heat source effects.

Marangoni convection, induced by a surface tension gradient at the interface, is an important physical phenomenon in conditions of microgravity. In the mid-1860s, Marangoni discovered the phenomenon whereby the gravity-dominated natural convection of the liquid gradually disappeared in an environment of microgravity, while at the interface of the liquid, surface tension plays an important role and causes a gradient. In general, the surface tension is assumed to vary with concentration and temperature in a linear relationship:

$$\sigma = \sigma_0(1 - \gamma_T(T - T_\infty) - \gamma_C(C - C_\infty)),\ \gamma_T = -\frac{1}{\sigma_0}\frac{\partial\sigma}{\partial T}\bigg|_T,\ \gamma_C = -\frac{1}{\sigma_0}\frac{\partial\sigma}{\partial C}\bigg|_C$$

where u and w are the velocities along z and r directions; $\Re$ is the characteristic radius of the disk, T is the temperature; C is the nanoparticle volume fraction (NVF); A and B are characteristic temperature and nanoparticles volume fraction at the disk surface, respectively; T_∞ and C_∞ are, respectively, the ambient temperature and nanoparticle volume fraction; D_B is the coefficient of Brownian diffusion; D_T is the coefficient of thermophoretic diffusion; Q_e and Q_t are, respectively, the coefficients of ESHS and THS, λ_T and λ_C are the thermal and solutal relaxation time, respectively; τ is the specific heat ratio; k, ν, μ, ρ, δ, and c_p are the kinematic viscosity, thermal conductivity, dynamic viscosity, density, electrical conductivity, and specific heat, respectively; B_0 is the magnetic induction; β_c and n are the dimensionless Casson material parameter and dimensionless exponential index, respectively; σ is the surface tension; and $\sigma_0 > 0$ is constant.

3. Solution Procedure

The governing partial differential system (PDE) is solved numerically using the similarity method. The similarity approach identifies equations for which solutions depend on a certain group of independent variables rather than each one. This technique helps to transform the PDE's (partial differential equations) into ODE's (ordinary differential equations). Transformed ODE's are then solved using the Finite difference method together with the Richardson extrapolation-based dsolve routine. Now consider the following Von Karman transformations [45]:

$$\begin{gathered} u = r\Omega F(\xi),\ \ w = \sqrt{\Omega\nu}H(\xi),\ \ T = T_\infty + A\left(\tfrac{r}{\Re}\right)^2\theta(\xi), \\ C = C_\infty + B\left(\tfrac{r}{\Re}\right)^2\phi(\xi), \xi = \tfrac{z}{r}\sqrt{Re} \end{gathered} \tag{6}$$

The reduced ODE system is,

$$2F + H' = 0 \tag{7}$$

$$\left(1 + \frac{1}{\beta_c}\right)F'' - F(Ha + F) - F'H = 0 \tag{8}$$

$$\begin{gathered} \tfrac{1}{Pr}\theta'' + Nb\theta'\phi' + Nt(\theta')^2 + Q_E exp\{-n\xi\} + Q_T\theta - 2F\theta - H\theta' \\ -\alpha\left[4F^2\theta + H\theta'(4F + H') + H(H\theta'' + 2\theta F')\right] = 0 \end{gathered} \tag{9}$$

$$\begin{gathered} \phi'' + \tfrac{Nt}{Nb}\theta'' - LePr(2F\phi + H\phi') \\ -\beta LePr\left[4F^2\phi + H\phi'(4F + H') + H(H\phi'' + 2\phi F')\right] = 0 \end{gathered} \tag{10}$$

$$\begin{gathered} \left(1 + \tfrac{1}{\beta_c}\right)F'(0) = -2Ma(1 + R),\ H(0) = 0,\ \theta(0) = 1,\ \phi(0) = 1, \\ F(\infty) \to 0,\ \theta(\infty) \to 0,\ \phi(\infty) \to 0 \end{gathered} \tag{11}$$

The following are the non-dimensional parameters:

$Pr = \frac{\nu(\rho c_p)}{k}$ denotes Prandtl number, $Nt = \frac{\tau D_T(T_w - T_\infty)}{\nu T_\infty}$ denotes thermophoresis number, $Ha = \frac{\delta B_0^2}{\rho\Omega}$ denotes Hartmann number, $Nb = \frac{\tau D_B(C_w - C_\infty)}{\nu}$ denotes Brownian motion number, $Q_E = \frac{Q_e}{\rho c_p\Omega}$ denotes exponential space-dependent heat source number (ESHS), $Q_T = \frac{Q_t}{\rho c_p\Omega}$ denotes thermal-dependent heat source number (THS), $Le = \frac{k}{D_B(\rho c_p)}$ denotes Lewis number, $R = \frac{\gamma_C B}{\gamma_T A}$ denotes Marangoni ratio number, $Ma = \frac{\sigma_0\gamma_T A}{\Re^2\mu\Omega}\sqrt{\frac{\nu}{\Omega}}$

denotes Marangoni number, $\alpha = \lambda_T \Omega$ denotes the thermal relaxation parameter, and $\beta = \lambda_C \Omega$ denotes the solutal relaxation parameter.

The local Sherwood and Nusselt numbers are given below:

$$Sh = \frac{-r\left(\frac{\partial C}{\partial z}\right)_{z=0}}{C_w - C_\infty}, \tag{12}$$

$$Nu = \frac{-r\left(\frac{\partial T}{\partial z}\right)_{z=0}}{T_w - T_\infty}. \tag{13}$$

The non-dimensional form of (12)–(13) are:

$$Sh_r = \frac{Sh}{\sqrt{Re}} = -\phi'(0), \tag{14}$$

$$Nu_r = \frac{Nu}{\sqrt{Re}} = -\theta'(0). \tag{15}$$

where $Re = \frac{r^2\Omega}{\nu}$ is the local Reynolds number.

The Equations (7)–(11) are nonlinear and coupled in nature. The analytical solution of these equations can't be guaranteed and, hence, they are solved by FDM along with Richardson extrapolation using dsolve command in MAPLE. Further, obtained FDM results are compared with those estimated by bvp5c method. The comparison values of $F'(1)$ are tabulated in Table 1 and an excellent agreement is established.

Table 1. Comparison of $F'(1)$ values obtained by FDM and bvp5c method when β_c = 0.5 and $\xi_{max} = 8$.

Ha	**Ma**	**R**	**Finite Difference Method (FDM)**	**MATLAB bvp5c Method**	**Absolute Difference**
0.5	0.5	0.4	−0.216620	−0.216620	0.000000
0.7			−0.206954	−0.206954	0.000000
0.9			−0.198161	−0.198162	0.000001
1.1			−0.190115	−0.190116	0.000001
1.3			−0.182713	−0.182714	0.000001
	0.1		−0.050179	−0.050180	0.000001
	0.2		−0.095904	−0.095904	0.000000
	0.3		−0.138483	−0.138484	0.000001
	0.4		−0.178583	−0.178583	0.000000
	0.5		−0.216620	−0.216620	0.000000
		0.2	−0.216620	−0.216620	0.000000
		0.4	−0.246955	−0.246955	0.000000
		0.6	−0.276190	−0.276190	0.000000
		0.8	−0.304428	−0.304429	0.000001
		1.0	−0.331755	−0.331756	0.000001

4. Results and Discussion

A comprehensive parametric analysis is implemented to examine the stimulus of key parameters on axial velocity (F), radial velocity (H), temperature (θ), and NVF (ϕ). Figure 2a–d illustrates the impact of the magnetic parameter ($0 \leq H\alpha \leq 0.9$) on axial velocity (F), radial velocity (H), temperature (θ), and NVF (ϕ). The magnetic field tempts the retarding body force (so-called the Lorentz force) which reduces the flow and causes an upsurge in the thickness of the thermal and solute boundary layers. The electrically conductive fluid, under the Lorentz force perpendicular to the disk, creates the maximum resistance to flow, which implies a decrease in the axial velocity while observing the opposite behavior for the radial velocity. Dhanai et al. [8] reported similar results for the applied magnetic field. Furthermore, the results of Nadeem et al. [16], Eldabe et al. [17], and Lin et al. [26] are in agreement with our results. Lin et al. [26] concluded that the applied magnetic field could be used to control the rheology of working fluids in various industrial applications.

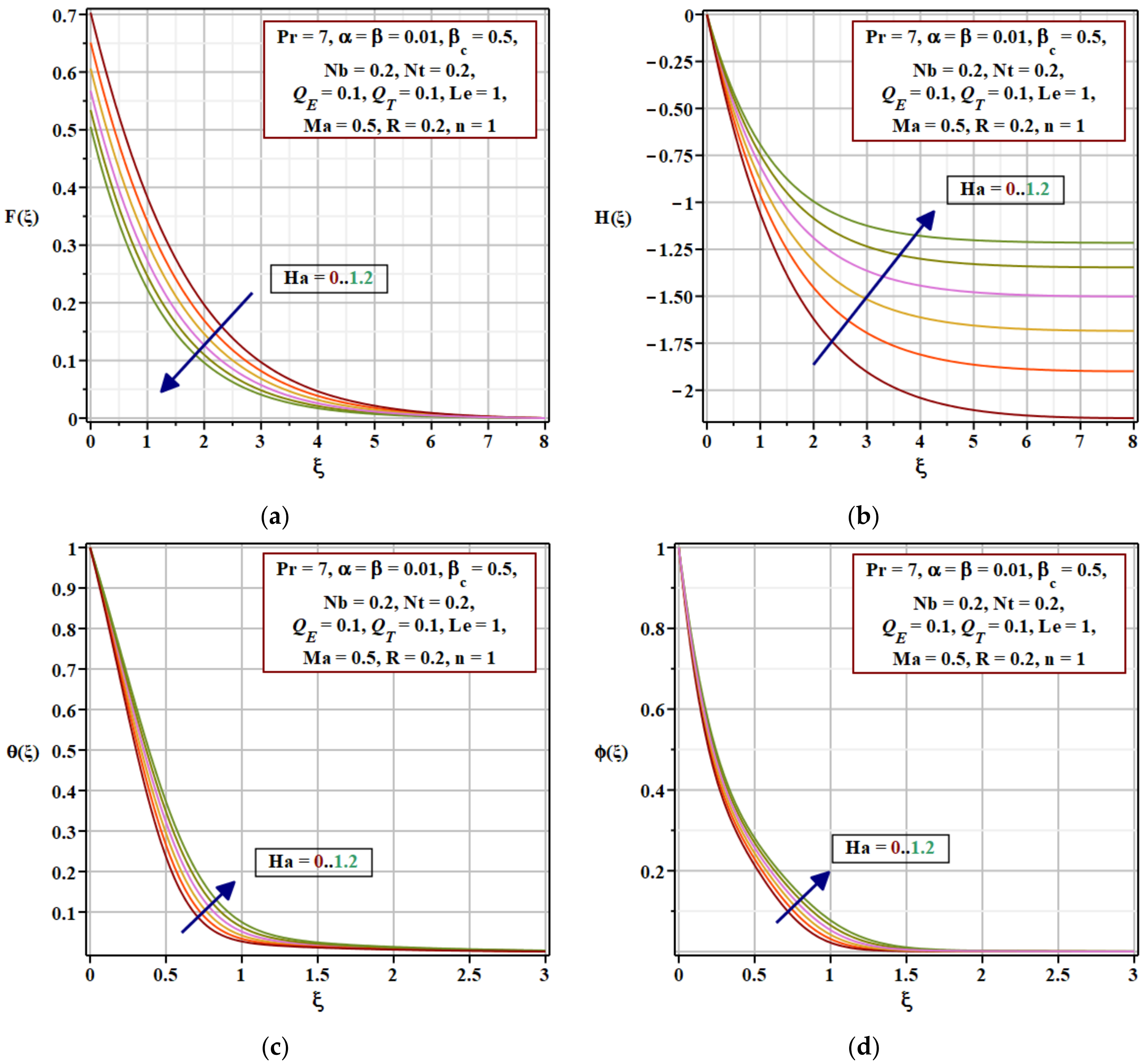

Figure 2. (**a**) $F(\xi)$, (**b**) $H(\xi)$, (**c**) $\theta(\xi)$, and (**d**) $\phi(\xi)$ for different values of *Ha*.

Figure 3a–d depicts the stimulus of the Marangoni number (Ma) on the $F(\xi)$, $H(\xi)$, $\theta(\xi)$ and $\phi(\xi)$. It illustrated that an increase in Ma leads to an abundance of radial flow, thereby increasing the radial velocity and decreasing the azimuth velocity. The thermal surface layer thickness shrinks as *Ma* upsurges, this is due to the reduction in thermal diffusion that occurs as *Ma* escalates. Similar to the thermal layer, the solute layer also falls as *Ma* increase. The effect of Marangoni ratio parameter on $F(\xi)$, $H(\xi)$, $\theta(\xi)$, and $\phi(\xi)$ is depicted in Figure 4a–d. The outcomes of the Marangoni ratio parameter (R) and Marangoni number are qualitatively similar. As can be seen, the Marangoni ratio parameter (R) appears in the velocity boundary condition $\left(1+\frac{1}{\beta_c}\right)F'(0) = -2M(1+R)$, as a factor of Marangoni number Ma. Thereby, the consequences of the Marangoni ratio parameter on the flow system are similar to those of the Marangoni number (Ma). The results of the Marangoni parameter are in collaboration with those reported by Ibrahim [27], Mahanta et al. [29], and Wahid et al. [46].

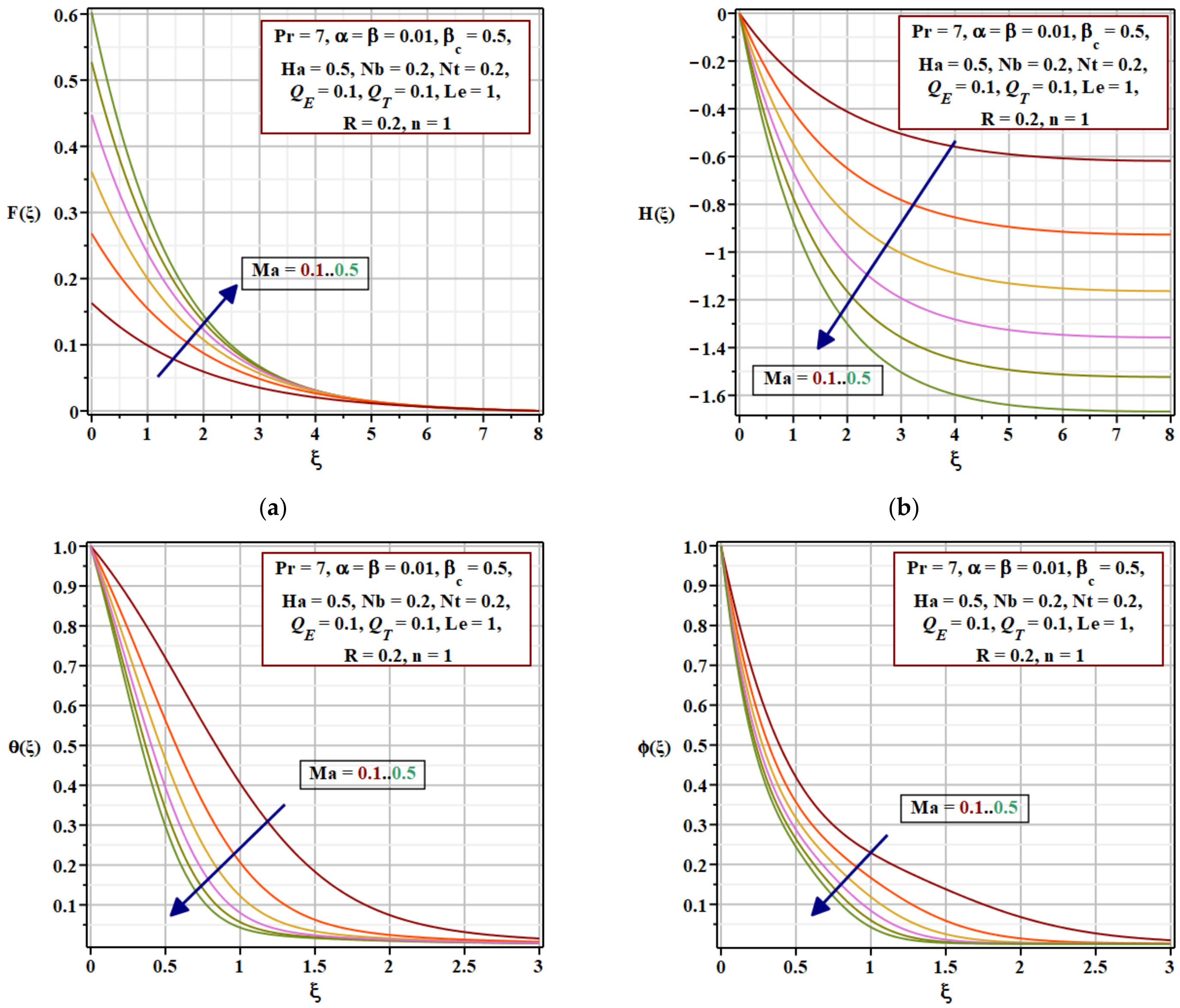

(**a**) (**b**) (**c**) (**d**)

Figure 3. (**a**) $F(\xi)$, (**b**) $H(\xi)$, (**c**) $\theta(\xi)$, and (**d**) $\phi(\xi)$ for different values of Ma.

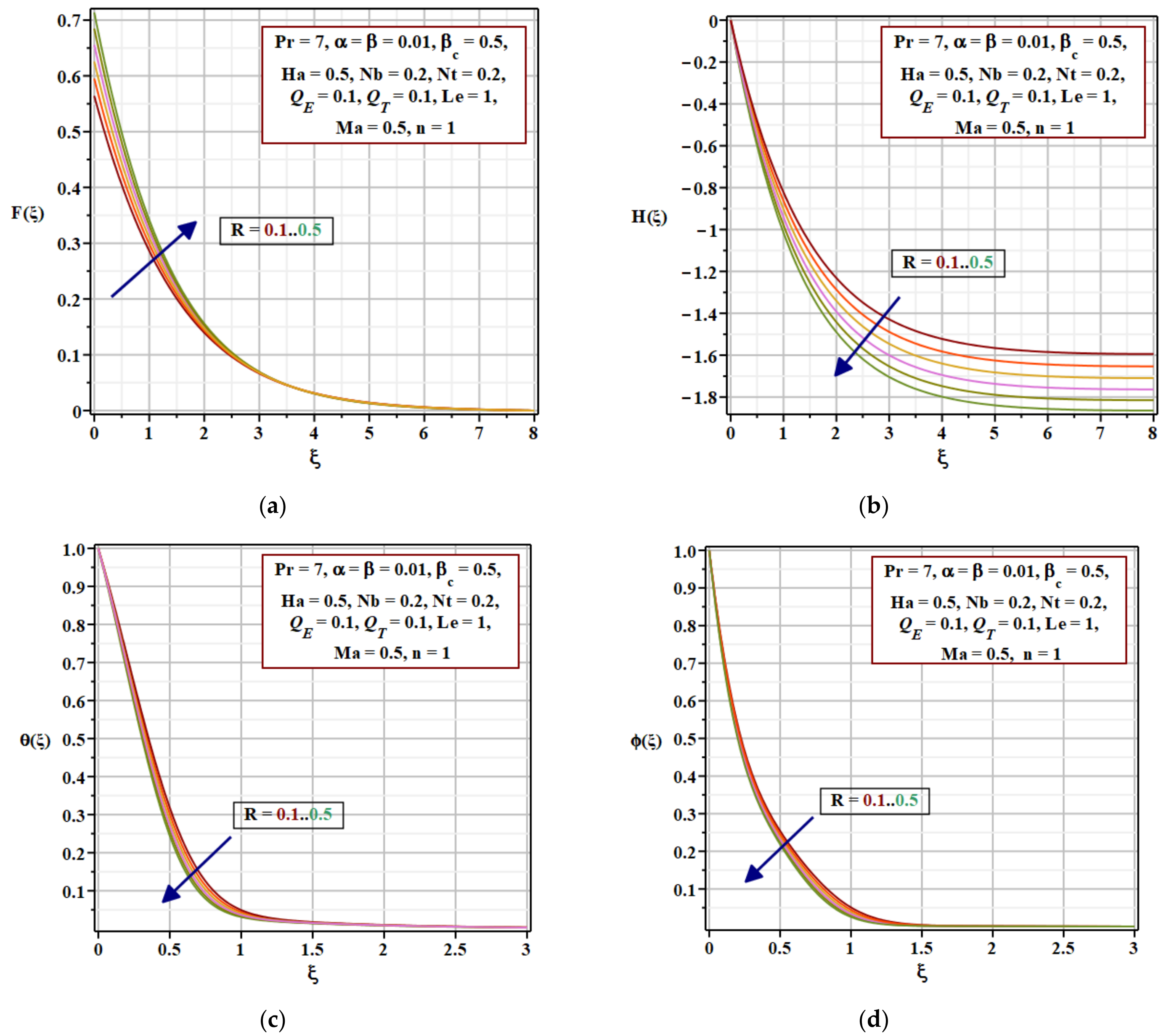

Figure 4. (**a**) $F(\xi)$, (**b**) $H(\xi)$, (**c**) $\theta(\xi)$, and (**d**) $\phi(\xi)$ for different values of R.

Brownian motion is the random and uncontrolled movement of particles in a fluid when they constantly collide with other molecules [3]. Buongiorno [3] also described that random Brownian motion results in the net movement of solute or suspended particles from regions of higher concentration to regions of lower concentration, a process called diffusion. Therefore, diffusion acts in opposition to centrifugal sedimentation, which tends to concentrate the particles. Brownian motion causes the arbitrary motion of nanoparticles within the working fluid. Therefore, the increase in the *Nb* causes a chaotic movement of the particles which affects the heat transfer positively. This mechanism is shown in Figure 5a, while this random movement of the nanoparticles reduces the solute field (see Figure 5b). Nield and Kuznetsov [4] also reported that the Brownian motion factor is favorable to the growth of the thermal boundary layer, while Brownian motion has a very limited effect on the Nusselt number. Our Brownian motion results are similar to those reported by Rana and Bhargava [6]. Another technique for improving thermal energy transfer is the thermophoresis mechanism, in which an increase in thermal energy is achieved by providing additional energy to the system through the thermal gradient.

Therefore, the increase in *Nt* significantly increases the thermal and solute layer, as can be seen in Figure 6a,b. The effect of the thermophoresis number on the thermal field (Nusselt number) is also more evident than that of the Brownian motion parameter. Kuznetsov and Nield [7] report a similar observation, that is, the thermophoresis factor influences the Nusselt number with a rate of 0.1052 while the Brownian motion parameter influences the Nusselt number with a rate of 0.0001.

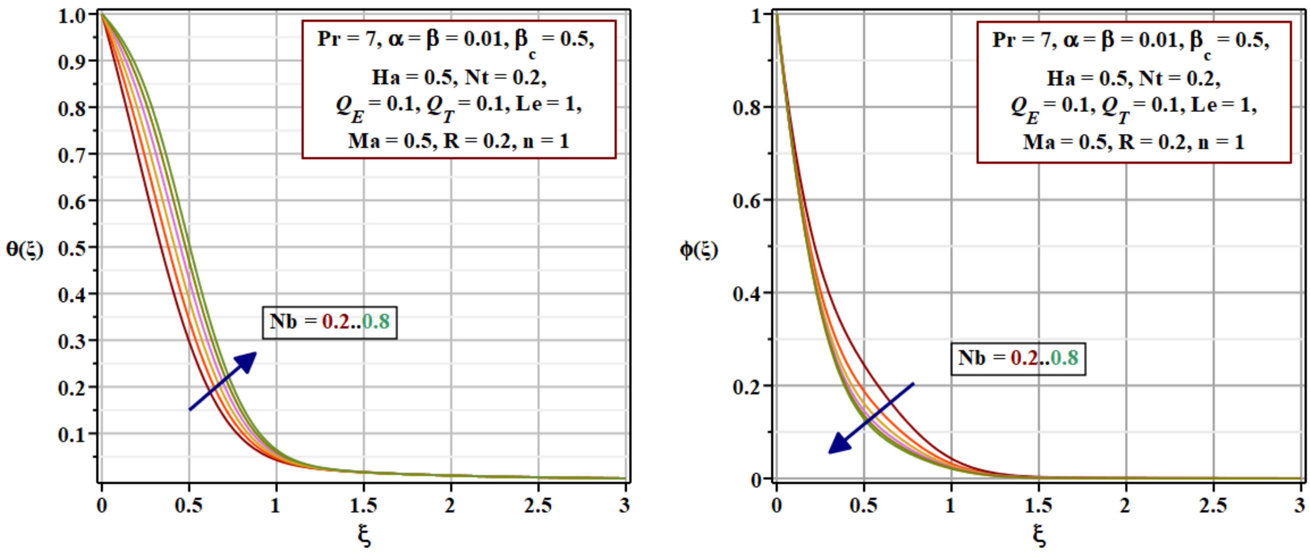

(**a**) (**b**)

Figure 5. (**a**) $\theta(\xi)$ and (**b**) $\phi(\xi)$ for different values of *Nb*.

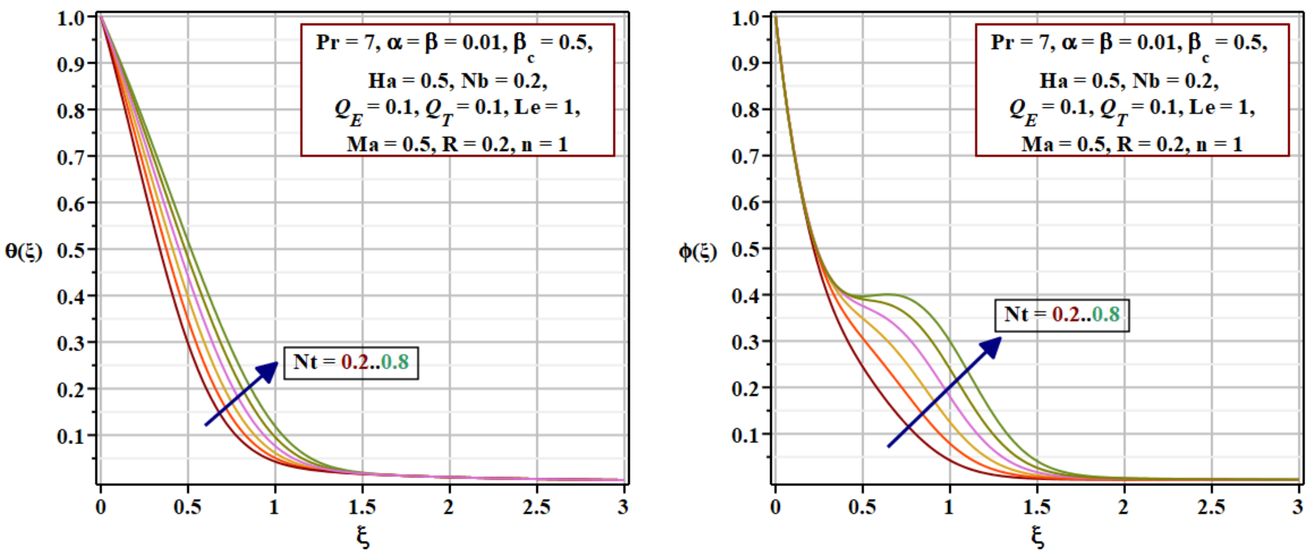

(**a**) (**b**)

Figure 6. (**a**) $\theta(\xi)$ and (**b**) $\phi(\xi)$ for different values of *Nt*.

The *Le* relates to both thermal and mass diffusivity. The physical mechanism of the Lewis number on heat and mass flow can be seen in Figure 7a,b. Figure 7a portrays the downturn in the thermal boundary layer and Figure 7b shows a significant reduction in the NVF layer thickness as *Le* increases i.e., the attenuation of mass diffusivity. Our Lewis number results are similar to those reported by Rana and Bhargava [6], and Kuznetsov and Nield [7].

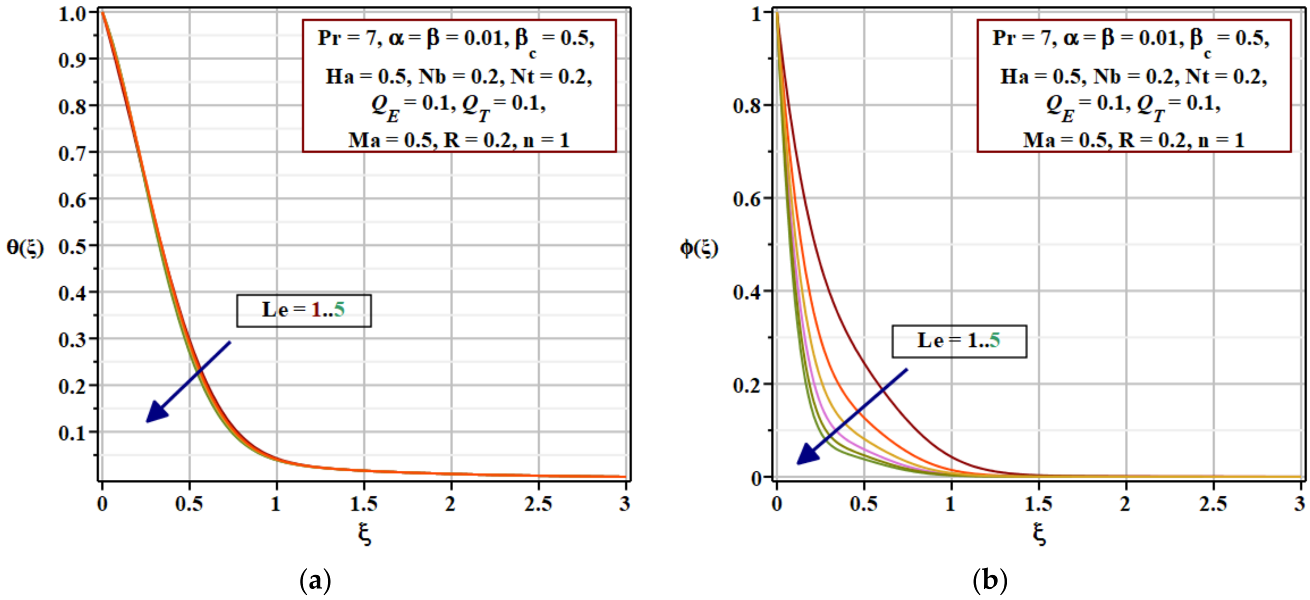

Figure 7. (**a**) $\theta(\xi)$ and (**b**) $\phi(\xi)$ for different values of *Le*.

The significance of two distinct thermal energy modulations (ESHS and THS) on $\theta(\xi)$ and $\phi(\xi)$ is explained pictorially in Figures 8 and 9. An increase in Q_E and Q_T yields an extra heat in the system, which leads to an increase in the thermal field, whereas increasing values of the Q_E and Q_T leads to a dual behavior in the $\phi(\xi)$. Amongst two different thermal energy modulations, namely ESHS and THS, ESHS is more significant for solar thermal applications which encompass the heating process. The current results of ESHS and THS parameters are in agreement with our previous findings [19].

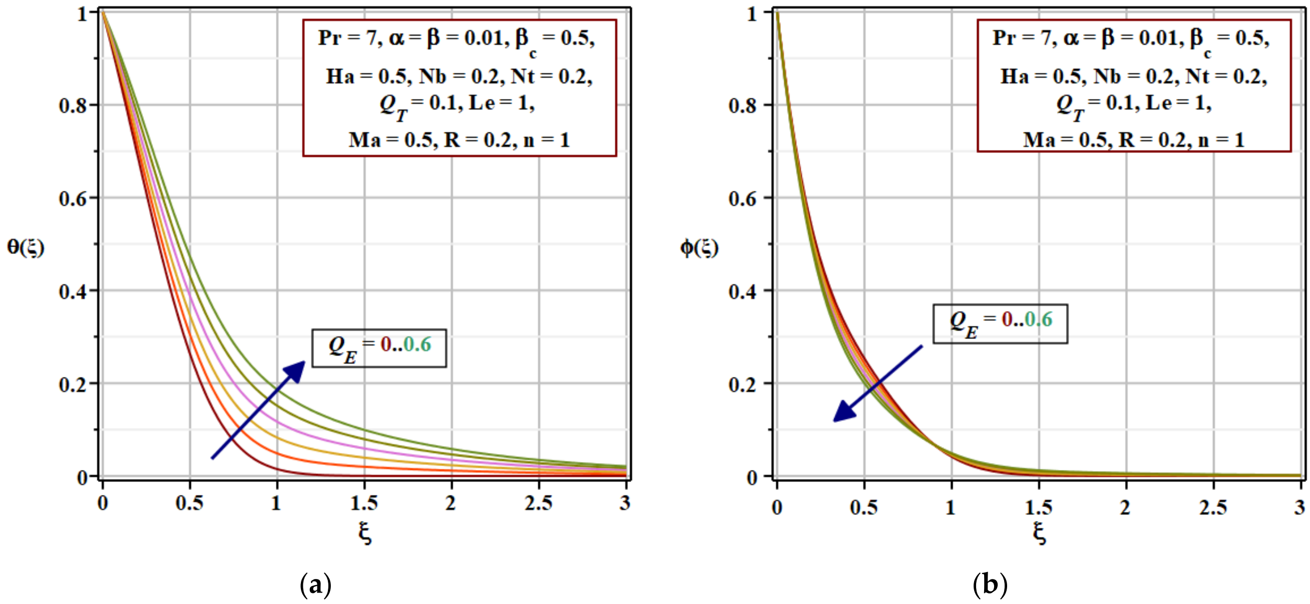

Figure 8. (**a**) $\theta(\xi)$ and (**b**) $\phi(\xi)$ for different values of Q_E.

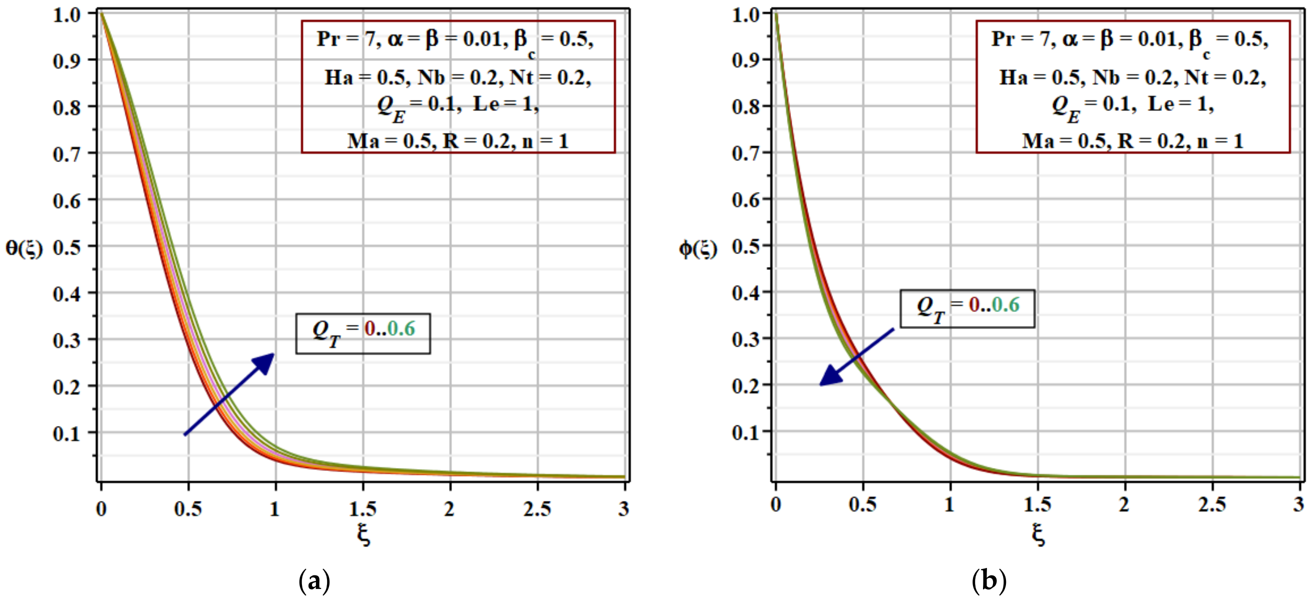

Figure 9. (**a**) $\theta(\xi)$ and (**b**) $\phi(\xi)$ for different values of Q_T.

Three-Dimensional surface and columns plots are utilized to analyze the influence of key parameters on the Nusselt number (Nu_r) and Sherwood number (Sh_r) (see Figure 10a–e). It is observed that the higher the Nb and Nt, the lower the heat transfer rate Nu_r. This is because the thermal layer thickness is wider for larger values of both Nb and Nt. Similarly, Nu_r inversely responses to Q_E and Q_T. As ESHS and THS modulations improve the thickness of the thermal layer structure, the heat transfer rate is reduced for larger Q_E and Q_T. Therefore, to achieve the maximum heat transfer rate, both Q_E and Q_T must be kept as low as possible. Higher values of Hartman number ($H\alpha$) and Lewis number (Le) lead to significant heat transfer. The maximum heat transfer rate Nu_r is found when both Marangoni number and Marangoni ratio parameters are kept at higher values. Therefore, the Marangoni convection process is vital in thermal energy systems. The higher the α and the lower the β, the higher the heat transfer rate.

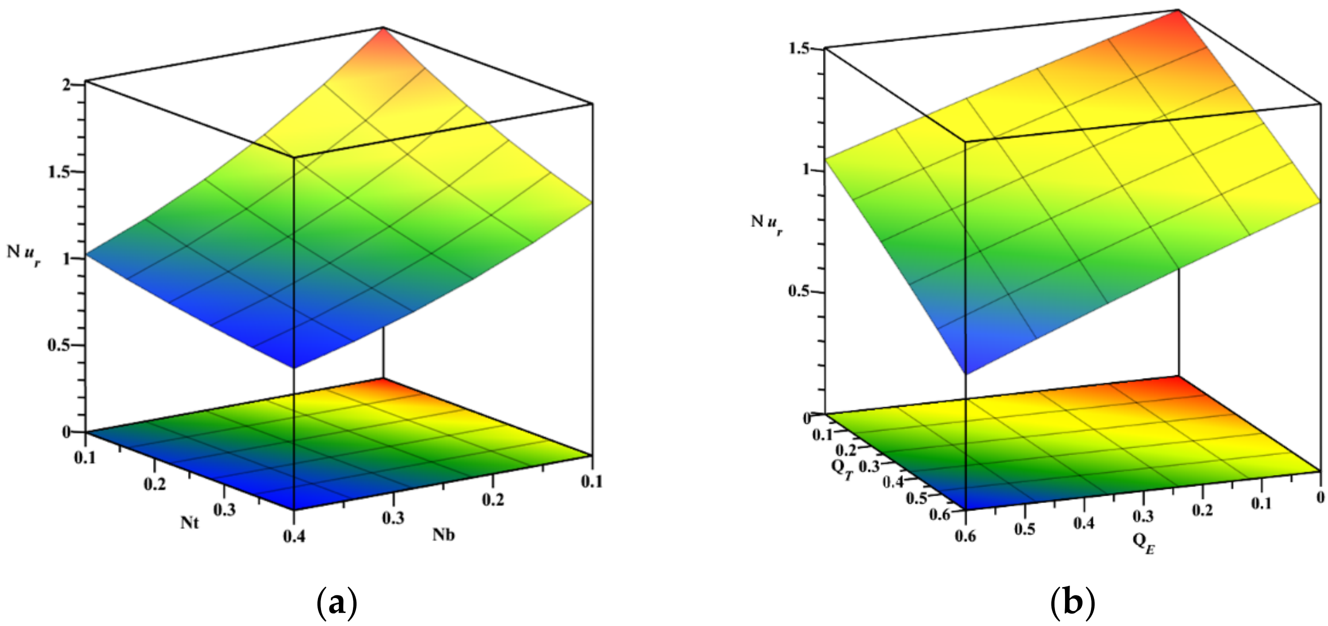

Figure 10. *Cont.*

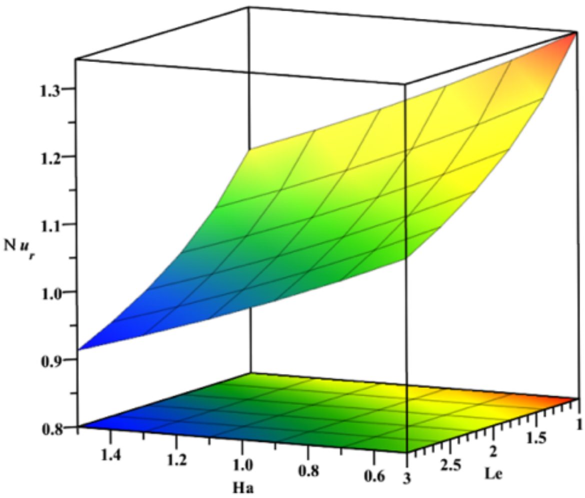

(**c**)

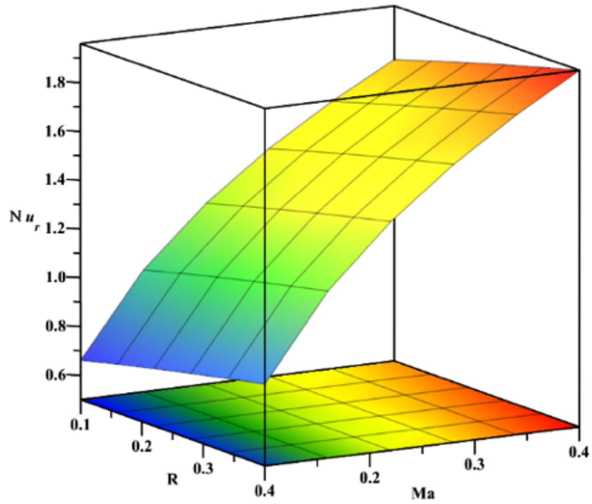

(**d**)

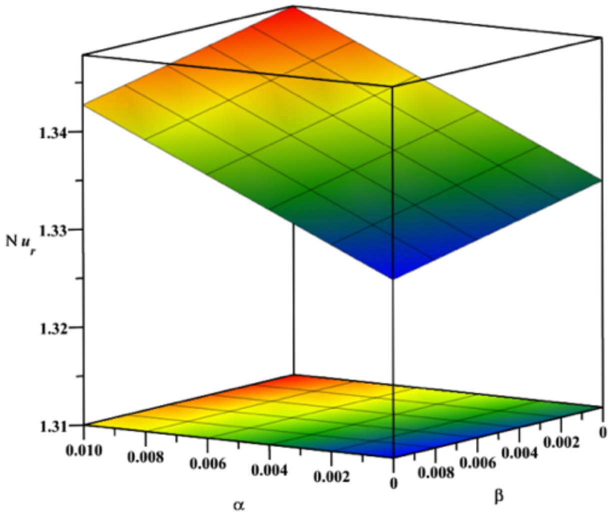

(**e**)

Figure 10. (**a**–**e**): The surface plots of reduced Nusselt number Nu_r.

The impact of the key parameters on the Sherwood number (Sh_r) is represented by 3D column plots (see Figure 11a–d). The maximum Sherwood number (Sh_r) is found for higher Le and lower Ha. Figure 11b depicts that Sh_r will increase for increasing values of Nb and decreasing values of Nt. For the large values of Ma and R, the Sherwood number (Sh_r) is increased (see Figure 11c). This is because both Ma and R improve the solute layer structure. Similar behavior is observed for the ESHS and THS mechanisms (see Figure 11d).

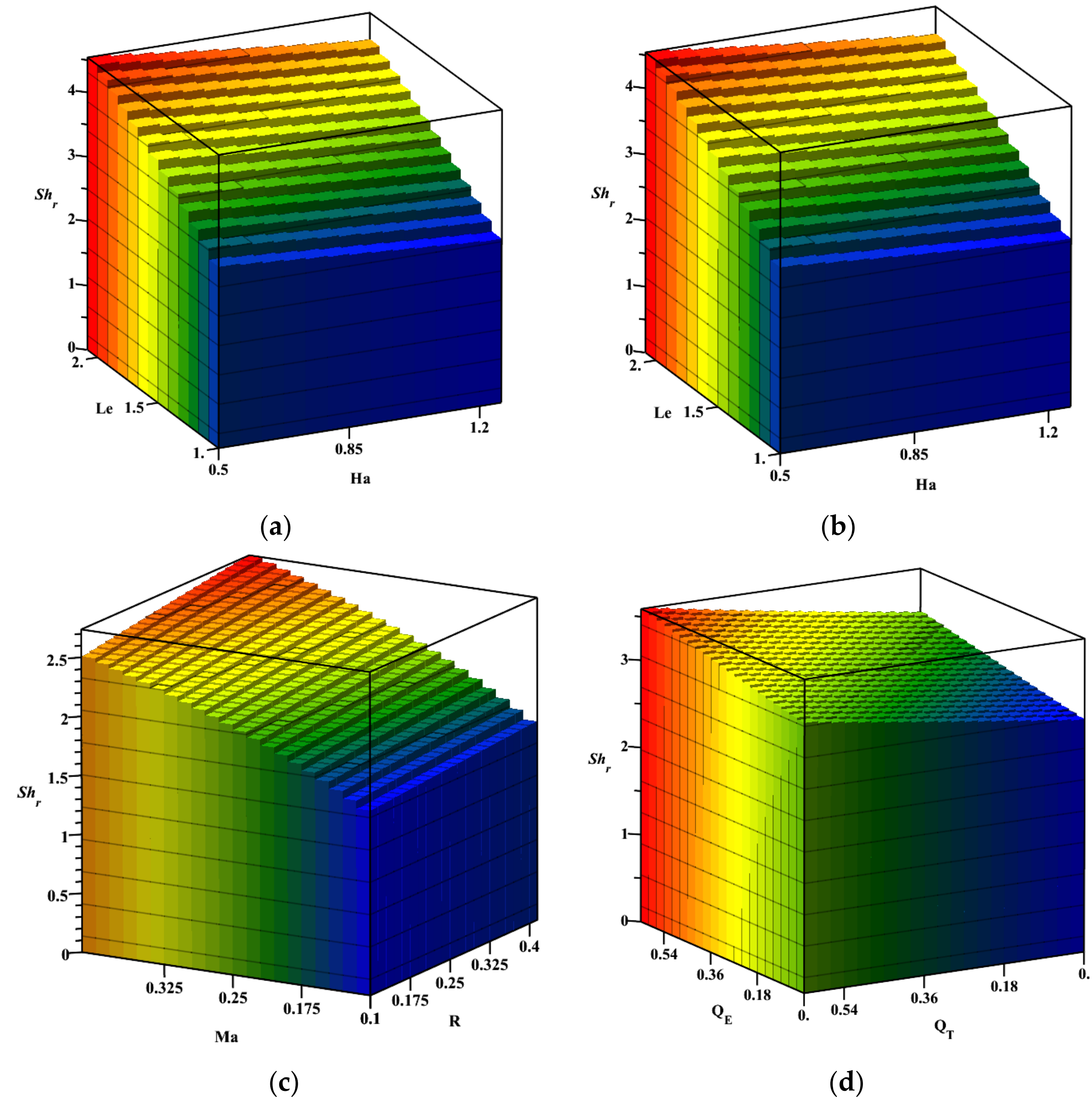

Figure 11. (**a**–**d**): The histograms of reduced Sherwood number Sh_r.

5. Correlations

Regression correlations can be used to assess the strength of the relationship between variables and to predict the future relationship between them. Regression computation includes several types, such as linear, multiple linear, logarithmic, and non-linear. Linear and multiple linear models are most common. Nonlinear regression analysis is commonly used for more complex datasets where the dependent and independent variables show a nonlinear relationship. The different correlation models are computed for the Nusselt number for two different sets of physical parameters to analyze the results. Firstly, Nu_{est} is estimated for 169 sets of values of Nb and Nt in the range $0.1 \leq Nb, Nt \leq 0.4$. Linear, quadratic, and logarithmic regressions were performed on the results, and they are given below:

Linear model:

$$Nu_{est} = -2.893664\,Nb - 1.168271\,Nt + 2.078968,\ \text{with } R^2 = 95.87\%\text{ and residual standard error } 0.0607883 \quad (16)$$

Quadratic model:

$$Nu_{est} = -6.607731Nb - 3.241193Nt + 4.933011Nb^2 + 1.650721Nt^2 + 4.990246NbNt + 2.7447342,\ \text{with } R^2 = 99.89\%\text{ and residual standard error } 0.009936 \quad (17)$$

Logarithmic model:

$$Nu_{est} = -0.649939\ln Nb - 0.261244\ln Nt - 0.273526,\ \text{with } R^2 = 97.41\%\text{ and residual standard error } 0.0481435 \quad (18)$$

Equation (16) implies that an increase in both Nb and Nt leads to a decrease in Nu_{est}. These results are consistent with our graphical results (see Figure 10a). However, the interactive and quadratic effects of Nb and Nt are favorable for Nu_{est} (see Equation (17)). Further, the quadratic model has a more precise fit for the Nusselt number than the linear and logarithmic models.

This exercise was reiterated to present the models for Nu_r and Sh_r as a function of Nb, Nt, Ma, and Q_E. Now Nu_r and Sh_r are estimated for 1296 sets of values of Nb, Nt, Ma, and Q_E in the range $0.1 \le Nb, Nt \le 0.4$, $0.1 \le Ma \le 0.5$, and $0 \le Q_E \le 0.4$. The linear and quadratic regressions were performed on the outcome and recorded in Table 2.

Table 2. Correlations for Nu_{est} and Sh_{est}.

Correlations for Nu_{est}				
Type	**Model**			
Linear	$1.945542Ma - 1.020937Q_E - 1.960794Nb - 0.775818Nt + 0.975552$			
	Adjusted R^2	90.9%	**Residual Standard Error**	0.117025
Quadratic	$3.517448Nb^2 + 1.076601Nt^2 - 0.191755Q_E^2 - 3.442968Ma^2 + 3.372623NbNt - 1.801812MaNt + 2.075881NbQ_E + 1.817708MaQ_E + 4.098234Ma - 2.008518Q_E - 4.977851Nb - 1.616731Nt + 1.2532640$			
	Adjusted R^2	96.22%	**Residual Standard Error**	0.075439
Correlations for Sh_{est}				
Type	**Model**			
Linear	$4.741571Ma + 0.509317Q_E + 1.206153Nb + 0.465005Nt + 1.509320$			
	Adjusted R^2	93.50%	**Residual Standard Error**	0.175312
Quadratic	$0.624259Nt^2 - 8.412765Nb^2 - 5.381747Ma^2 + 0.172606Q_E^2 + 0.838207NbNt - 0.797004MaNt - 3.985166NbQ_E - 1.503554MaQ_E + 8.470582Ma + 1.887632Q_E + 6.000017Nb + 0.182425Nt + 0.427243$			
	Adjusted R^2	97.14%	**Residual Standard Error**	0.116279

Table 2 shows that an increase in Nb, Nt, $Q_{E,}$ and Ma leads to an increase in $Sh_{est.}$ However, the interactive effects of Nb and Nt are favorable for Sh_{est}. The Marangoni number is positively correlated to Nu_{est} and Sh_{est}. Furthermore, the quadratic model has a more accurate fit to both Nu_{est} and Sh_{est} than the linear model.

6. Concluding Remarks

The significance of two distinct thermal energy modulations in the Marangoni convective flow of nanomaterial across an infinite disk is examined numerically. The CCF is utilized in the thermal energy analysis. Several mathematical models for reduced Nusselt number and Sherwood number are proposed. Here are some key findings from this work:

- The strength of the Lorentzian body increases the thermal and solutal layer thickness but decreases the velocity. This is due to the retardation force exerted by the applied magnetic field.
- The Brownian motion and thermophoresis phenomena improve the heat transfer, but when it comes to the solute, the thermophoresis number increases the mass transfer and the opposite nature is observed for the Brownian number. This is due to the Brownian motion and thermophoresis mechanisms of nanoparticles.
- Thermal energy modulations (ESHS and THS) significantly improve the temperature field, as both modulations supply additional heat into the nanoliquid system.
- A decrease in the thickness of both the thermal and the solute layer is observed as the Lewis number increases.
- Marangoni convection progresses the velocity of the nanomaterial. This is due to the surface tension at the disk surface.
- The Nusselt number is higher in the presence of the Marangoni convection.
- The Nusselt number is found as a maximum for the effect of nanoparticles.
- Sherwood's number improved by increasing the Lewis number and heat source parameter.
- Quadratic regression is more important than the linear model for both the reduced Nusselt number and the Sherwood number

Author Contributions: Conceptualization, M.B. and G.L.; methodology, S.N.; software, S.N.; validation, A.A., T.M. and M.B.; formal analysis, M.B.; investigation, G.L.; resources, A.A.; data curation, T.M.; writing—original draft preparation, S.N.; writing—review and editing, M.B. and G.L.; visualization, T.M.; supervision, T.M.; project administration, T.M.; funding acquisition, G.L. All authors have read and agreed to the published version of the manuscript.

Funding: This research received no external funding.

Institutional Review Board Statement: Not applicable.

Informed Consent Statement: Not applicable.

Conflicts of Interest: The authors declare no conflict of interest.

Nomenclature

A	characteristic temperature (K)
B	characteristic nanoparticles volume fraction
B_0	magnetic field intensity (telsa)
C	Nanoparticles volume fraction
c_p	specific heat
C_∞	ambient nanoparticle volume fraction
C_w	nanoparticle volume fraction at the surface of the disk
D_B	coefficient of Brownian diffusion
D_T	coefficient of thermophoretic diffusion
F, H	dimensionless velocities along z and r direction
Ha	Hartmann number
k	Thermal conductivity
Le	Lewis number
Ma	Marangoni number
Nt	Thermophoresis number

Nb	Brownian motion number
Nu_r	reduced Nusselt number
Nu_{est}	estimated Nusselt number
n	dimensionless exponential index
Pr	Prandtl number
Q_e	coefficient of ESHS
Q_t	coefficient of THS
Q_E	dimensionless ESHS number
Q_T	dimensionless THS number
Re	Reynolds number
R	Marangoni ratio number
Sh_r	reduced Sherwood number
Sh_{est}	estimated Sherwood number
T	temperature
T_∞	ambient temperature
T_w	temperature at the surface of the disk
$\Re$	characteristic radius of the disk
u, w	velocities along z and r directions
Greek symbols	
α, β	nondimensional thermal and solutal relaxation parameter
β_c	dimensionless Casson material parameter
γ_C, γ_T	Constants
δ	electrical conductivity
θ	dimensionless temperature
λ_T	thermal relaxation time
λ_C	solutal relaxation time
μ	dynamic viscosity
ν	kinematic viscosity
ξ	Similarity variable
ρ	density
σ	surface tension
σ_0	constant
τ	specific heat ratio
ϕ	scaled nanoparticle volume fraction
Ω	constant (s^{-1})

References

1. Choi, S.U.S. Enhancing thermal conductivity of fluids with nanoparticles developments and applications of non-Newtonian fluid flow. *ASME FED* **1995**, *66*, 99–105.
2. Khanafer, K.; Vafai, K.; Lightstone, M. Buoyancy-driven heat transfer enhancement in a two-dimensional enclosure utilizing nanofluids. *Int. J. Heat Mass Transf.* **2003**, *46*, 3639–3653. [CrossRef]
3. Buongiorno, J. Convective transport in nanofluids. *ASME J. Heat Transf.* **2006**, *128*, 240–250. [CrossRef]
4. Nield, D.A.; Kuznetsov, A. Thermal instability in a porous medium layer saturated by a nanofluid. *Int. J. Heat Mass Transf.* **2009**, *5*, 5796–5801. [CrossRef]
5. Khan, W.A.; Pop, I. Boundary-layer flow of a nanofluid past a stretching sheet. *Int. J. Heat Mass Transf.* **2010**, *53*, 2477–2483. [CrossRef]
6. Rana, P.; Bhargava, R. Flow and heat transfer of a nanofluid over a nonlinearly stretching sheet: A numerical study. *Commun. Nonlinear Sci. Numer. Simul.* **2012**, *17*, 212–226. [CrossRef]
7. Kuznetsov, A.V.; Nield, D.A. The Cheng–Minkowycz problem for natural convective boundary layer flow in a porous medium saturated by a nanofluid: A revised model. *Int. J. Heat Mass Transf.* **2013**, *65*, 682–685. [CrossRef]
8. Dhanai, R.; Rana, P.; Kumar, L. MHD mixed convection nanofluid flow and heat transfer over an inclined cylinder due to velocity and thermal slip effects: Buongiornos model. *Powder Technol.* **2016**, *288*, 140–150. [CrossRef]
9. Mackolil, J.; Mahanthesh, B. Heat transfer optimization and sensitivity analysis of Marangoni convection in nanoliquid with nanoparticle interfacial layer and cross-diffusion effects. *Int. Commun. Heat Mass Transf.* **2021**, *126*, 105361. [CrossRef]
10. Mahanthesh, B. Flow and heat transport of nanomaterial with quadratic radiative heat flux and aggregation kinematics of nanoparticles. *Int. Commun. Heat Mass Transf.* **2021**, *127*, 105521. [CrossRef]

11. Skelland, H.P. *Non-Newtonian Flow and Heat Transfer*; John Wiley: Hoboken, NJ, USA, 1966.
12. Denn, M.M. Boundary-layer flows for a class of elastic fluids. *Chem. Eng. Sci.* **1967**, *22*, 395–405. [CrossRef]
13. Rajagopal, K.R.; Gupta, A.S.; Wineman, A.S. On a boundary layer theory for non-Newtonian fluids. *Appl. Sci. Eng. Lett.* **1980**, *18*, 875–883. [CrossRef]
14. Eldabe, N.T.M.; Elmohandis, S.M.G. Pulsatile Magnetohydrodynamic Viscoelastic Flow through a Channel Bounded by Two Permeable Parallel Plates. *J. Phys. Soc. Jpn.* **1995**, *64*, 4163–4174. [CrossRef]
15. Mustafa, M.; Hayat, T.; Pop, I.; Aziz, A. Unsteady boundary layer flow of a Casson fluid due to an impulsively started moving flat plate. *Heat Transf. Asian Res.* **2011**, *40*, 563–576. [CrossRef]
16. Nadeem, S.; Haq, R.U.; Lee, C. MHD flow of a Casson fluid over an exponentially shrinking sheet. *Sci. Iran.* **2012**, *19*, 1550–1553. [CrossRef]
17. Eldabe, N.T.M.; Saddeck, G.; El-Sayed, A.F. Heat transfer of MHD non-Newtonian Casson fluid flow between two rotating cylinders. *Mech. Mech. Eng.* **2001**, *5*, 237–251.
18. Gireesha, B.J.; Mahanthesh, B.; Rashidi, M.M. MHD boundary layer heat and mass transfer of a chemically reacting Casson fluid over a permeable stretching surface with non-uniform heat source/sink. *Int. J. Ind. Math.* **2015**, *7*, 247–260.
19. Mahanthesh, B.; Gireesha, B.J.; Shashikumar, N.S.; Hayat, T.; Alsaedi, A. Marangoni convection in Casson liquid flow due to an infinite disk with exponential space dependent heat source and cross-diffusion effects. *Results Phys.* **2018**, *9*, 78–85. [CrossRef]
20. Sohail, M.; Shah, Z.; Tassaddiq, A.; Kumam, P.; Roy, P. Entropy generation in MHD Casson fluid flow with variable heat conductance and thermal conductivity over non-linear bi-directional stretching surface. *Sci. Rep.* **2020**, *10*, 12530. [CrossRef]
21. Oke, A.; Mutuku, W.; Kimathi, M.; Animasaun, I. Insight into the dynamics of non-Newtonian Casson fluid over a rotating non-uniform surface subject to Coriolis force. *Nonlinear Eng.* **2020**, *9*, 398–411. [CrossRef]
22. Tufail, M.N.; Saleem, M.; Chaudhry, Q.A. Chemically reacting mixed convective Casson fluid flow in the presence of MHD and porous medium through group theoretical analysis. *Heat Transf.* **2020**, *29*, 4657–4677. [CrossRef]
23. Anwar, T.; Kumam, P.; Watthayu, W. Unsteady MHD natural convection flow of Casson fluid incorporating thermal radiative flux and heat injection/suction mechanism under variable wall conditions. *Sci. Rep.* **2021**, *11*, 4275. [CrossRef]
24. Zheng, L.; Zhang, X. Embedding-Parameters Perturbation Method. *Modeling Anal. Mod. Fluid Probl.* **2017**, 39–77. [CrossRef]
25. Pearson, J. On convection cells induced by surface tension. *J. Fluid Mech.* **1958**, *4*, 489–500. [CrossRef]
26. Lin, Y.; Zheng, L.; Zhang, X. Magnetohydrodynamics thermocapillary Marangoni convection heat transfer of power-law fluids driven by temperature gradient. *J. Heat Transf.* **2013**, *135*, 051702. [CrossRef]
27. Ibrahim, S.M. Effects of Mass Transfer, Radiation, Joule Heating, and Viscous Dissipation on Steady MHD Marangoni Convection Flow over a Flat Surface with Suction and Injection. *Int. J. Eng. Math.* **2013**, *2013*, 1–9. [CrossRef]
28. Mahanthesh, B.; Gireesha, B.J.; Shashikumar, N.S.; Shehzad, S.A. Marangoni convective MHD flow of SWCNT and MWCNT nanoliquids due to a disk with solar radiation and irregular heat source. *Phys. E Low Dimens. Syst. Nanostruct.* **2017**, *94*, 25–30. [CrossRef]
29. Mahanta, G.; Das, M.; Shaw, S.; Mahala, B.K. MHD Double-diffusive thermosolutal Marangoni convection non-Newtonian Casson fluid flow over a permeable stretchable sheet. *Heat Transf.* **2020**, *49*, 1788–1807. [CrossRef]
30. Shafiq, A.; Rasool, G.; Phali, L.; Khalique, C.M. Thermosoluted Marangoni convective flow towards a permeable Riga surface. *Open Phys.* **2020**, *18*, 535–544. [CrossRef]
31. Kármán, T.V. Über laminare und turbulente Reibung. *ZAMM* **1921**, *1*, 233–252. [CrossRef]
32. Turkyilmazoglu, M. MHD fluid flow and heat transfer due to a stretching rotating disk. *Int. J. Therm. Sci.* **2012**, *51*, 195–201. [CrossRef]
33. Turkyilmazoglu, M. MHD fluid flow and heat transfer due to a shrinking rotating disk. *Comput. Fluids* **2014**, *90*, 51–56. [CrossRef]
34. Makinde, O.D.; Mahanthesh, B.; Gireesha, B.J.; Shashikumar, N.S.; Monaledi, R.L.; Tshehla, M.S. MHD Nanofluid Flow Past a Rotating Disk with Thermal Radiation in the Presence of Aluminum and Titanium Alloy Nanoparticles. *Defect Diffus. Forum* **2018**, *384*, 69–79. [CrossRef]
35. Shehzad, S.A.; Mabood, F.; Rauf, A.; Tlili, I. Forced convective Maxwell fluid flow through rotating disk under the thermophoretic particles motion. *Int. Commun. Heat Mass Transf.* **2020**, *116*, 104693. [CrossRef]
36. Rasool, G.; Shafiq, A.; Khalique, C.M. Marangoni forced convective Casson type nanofluid flow in the presence of Lorentz force generated by Riga plate. *Discret. Contin. Dyn. Syst. S* **2021**, *14*, 2517–2533. [CrossRef]
37. Rashid, U.; Baleanu, D.; Liang, H.; Abbas, M.; Iqbal, A.; Rahman, J.U. Marangoni Boundary Layer Flow and Heat Transfer of Graphene–Water Nanofluid with Particle Shape Effects. *Processes* **2020**, *8*, 1120. [CrossRef]
38. Cattaneo, C. Sulla conduzione del calore. *Atti Semin. Mat. Fis. Univ. Modena Reggio Emilia* **1948**, *3*, 83–101.
39. Christov, C.I. On frame indifferent formulation of the Maxwell—Cattaneo model of finite-speed heat conduction. *Mech. Res. Commun.* **2009**, *36*, 481–486. [CrossRef]
40. Straughan, B. Thermal convection with the Cattaneo—Christov model. *Int. J. Heat Mass Transf.* **2010**, *53*, 95–98. [CrossRef]
41. Ahmad Khan, J.; Mustafa, M.; Hayat, T.; Alsaedi, A. Numerical Study of Cattaneo-Christov Heat Flux Model for Viscoelastic Flow Due to an Exponentially Stretching Surface. *PLoS ONE* **2015**, *10*, e0137363. [CrossRef] [PubMed]
42. Khan, M.I.; Alzahrani, F. Transportation of heat through Cattaneo-Christov heat flux model in non-Newtonian fluid subject to internal resistance of particles. *Appl. Math. Mech.* **2020**, *41*, 1157–1166. [CrossRef]

43. Gireesha, B.J.; Shankaralingappa, B.M.; Prasannakumar, B.C.; Nagaraja, B. MHD flow and melting heat transfer of dusty Casson fluid over a stretching sheet with Cattaneo–Christov heat flux model. *Int. J. Ambient. Energy* **2020**. [CrossRef]
44. Kareem, R.S.; Abdulhadi, A.M. A study of MHD and Darcy-Forchheimer effects on third grade flow with Cattaneo-Christov heat flux. *AIP Conf. Proc.* **2020**, *2292*, 020001. [CrossRef]
45. Kármán, T.V. Uberlaminare und turbulence reibung. *Z. Für Angew. Math. Und Mech.* **1921**, *52*, 233–252. [CrossRef]
46. Wahid, N.S.; Arifin, N.M.; Khashiie, N.S.; Pop, I. Marangoni hybrid nanofluid flow over a permeable infinite disk embedded in a porous medium. *Int. Commun. Heat Mass Transf.* **2021**, *126*, 105421. [CrossRef]